Supporting Information

Efficient Deep-Blue Electroluminescence from an Ambipolar Fluorescent Emitter in a Single-Active-Layer Device

Alison L. Fisher,[†] Katharine E. Linton,[‡] Kiran T. Kamtekar,[‡] Christopher Pearson,[†] Martin R. Bryce,[‡] Michael C. Petty[†]

[†]*School of Engineering and*
[‡]*Department of Chemistry and* [†,‡]*Centre for Molecular and Nanoscale Electronics, Durham University, Durham, DH1 3LE, UK*

Pages

S1-S6	Synthesis and Characterization
S7	^{1}H NMR Spectrum of Compound **2**
S8-S9	Cyclic voltammetric data
S9	Photophysical Studies: Absorption and Photoluminescence Spectra of Compounds **1** and **2**
S10-S11	Photoluminescence Spectra and Quantum Yield Measurements for Thin Films
S11-S14	Device Characterization and Measurements
S14-S16	DFT Calculations
S16-S17	References for the Supporting Information

Synthesis and Characterization: General Procedures

All air-sensitive reactions were conducted under a blanket of argon which was dried by passage through a column of phosphorus pentoxide. All commercial chemicals were used without further purification unless otherwise stated. Anhydrous toluene, tetrahydrofuran (THF) and diethyl ether (Et_2O) were dried through an HPLC column on an Innovative Technology Inc. solvent purification system. Column chromatography was carried out using 40-60 μm mesh silica. Analytical thin layer chromatography was performed on 20 mm pre-coated plates of silica gel (Merck, silica gel $60F_{254}$), visualization was made using ultraviolet light (254 nm). NMR spectra were recorded on: Bruker Avance-400, Varian Mercury-200, Varian Mercury-400, Varian Inova-500 and Varian VNMRS-700 spectrometers. Chemical shifts are reported in ppm relative to $CHCl_3$ as internal reference which was set to 7.26 ppm. Melting points were determined in open-ended capillaries using a Stuart Scientific SMP3 melting point apparatus at a ramping rate of 5 °C/min. Mass spectra were measured on a Waters Xevo OTofMS with an ASAP probe. Electron ionisation (EI) mass spectra were recorded on a Thermoquest Trace or a Thermo-Finnigan DSQ. Ion analyses were performed on a Dionex 120 Ion Chromatography detector. HPLC analysis was carried out using a PerkinElmer Series 200 HPLC instrument equipped with a diode array detector, usually monitoring at 254 nm. The column was a Phemonex HyperClone 5 μm ODS (C10) 120 Å, 250 x 4.6 mm; flow rate 1 mL min^{-1}.

Tapping mode AFM images of the films of **1** and **2** (Figure 5 in the text) were obtained using a Digital Instruments NanoMan II SPM.

SCHEME 1: Synthesis of Compound 2[a]

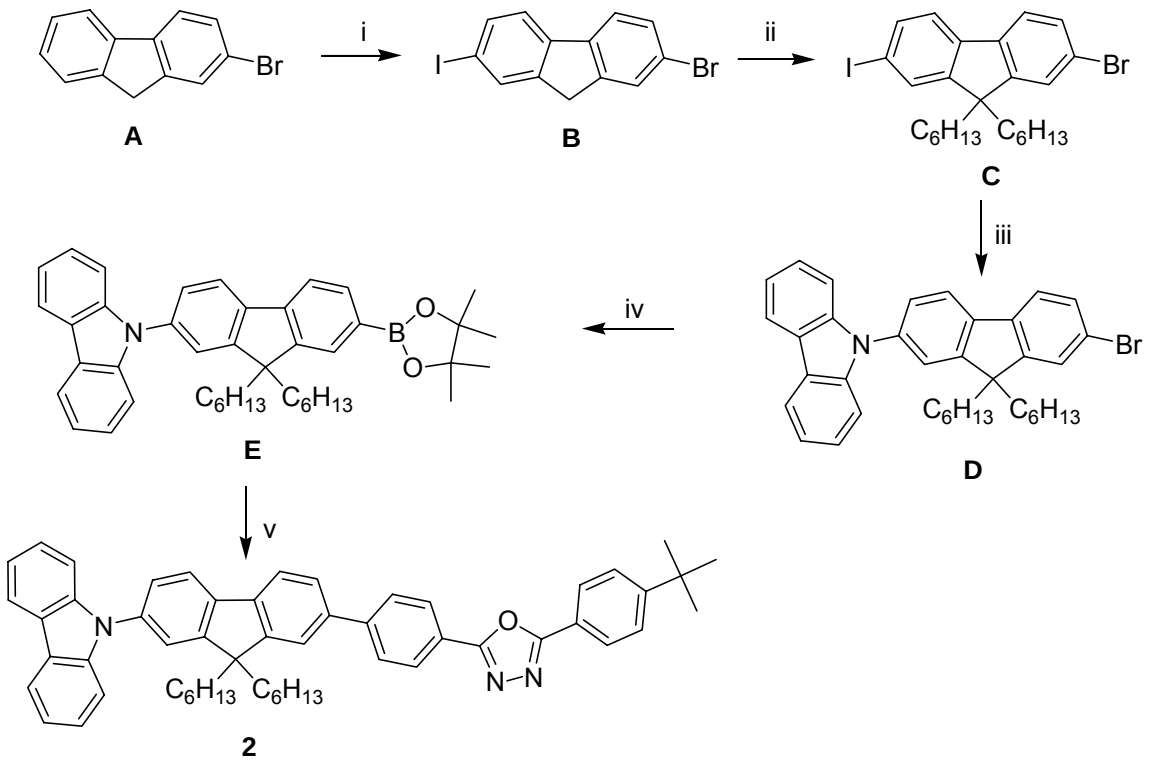

[a] i) AcOH, H_2SO_4, KIO_3, I_2, 80 °C, 18 h; ii) tetra-*n*-butylammonium chloride, NaOH, *n*-bromohexane, 20 °C, 20 h; iii) carbazole, CuI, 1,10-phenanthroline, K_2CO_3, DMF, 120 °C, 40 h; iv) *n*BuLi, 2-isopropoxy-4,4,5,5-tetramethyl-1,3,2-dioxaborolane, THF, -78 °C to 20 °C, 15 h; v) 2-(4-bromophenyl)-5-(4-*tert*-butylphenyl)-1,3,4-oxadiazole, $Pd(PPh_3)_2Cl_2$, NaOH (aq), THF, reflux, 15 h.

2-Bromo-7-iodo-9*H*-fluorene B

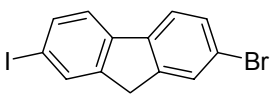

To a solution of 2-bromo-9*H*-fluorene **A** (16.00 g, 65.3 mmol) in glacial acetic acid (500 mL) and 20 % sulfuric acid (50 mL) potassium iodate (2.80 g, 13.1 mmol) followed by iodine (9.12 g, 35.9 mmol) were added. The reaction mixture was stirred at 80 °C for 18 h. The reaction mixture was then cooled, diluted with water (400 mL) and extracted with DCM (3 x 150 mL). The organic phase was washed with water (500 mL), aqueous $NaHCO_3$ (100 mL), brine solution (150 mL), dried over sodium thiosulfate, filtered and reduced. The solid was dissolved in DCM and the product precipitated with methanol. The product **B** was isolated as a white solid (15.80 g, 65%). NMR data were

consistent with the literature.[1] ^{1}H NMR ($CDCl_3$, 200 MHz) δ 7.93 – 7.85 (m, 1H), 7.76 – 7.57 (m, 3H), 7.57 – 7.43 (m, 2H), 3.87 (s, 2H).

2-Bromo-9,9-dihexyl-7-iodo-9*H*-fluorene C

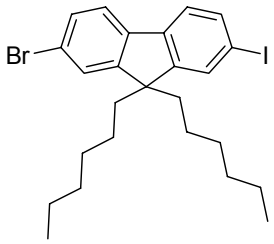

To a solution of **B** (15.80 g, 42.6 mmol) in DMSO (150 mL), tetra *n*-butylammonium chloride (2.0 g) was added followed by a solution of sodium hydroxide (4.26 g in 20 mL H_2O). To this stirred solution *n*-bromohexane was added. The reaction mixture was then stirred at room temperature for 20 h then extracted with ethyl acetate. The organic layers were washed with aqueous HCl, dried, filtered and concentrated. The crude product was purified by column chromatography on silica gel with 40 – 60 petroleum ether as eluent followed by recrystallization from ethanol. The product **C** was isolated as pale yellow crystals (15.6 g, 68%). The NMR data were consistent with the literature.[1] ^{1}H NMR ($CDCl_3$, 400 MHz) δ 7.70 – 7.57 (m, 2H), 7.56 – 7.47 (m, 1H), 7.47 – 7.34 (m, 3H), 1.97 – 1.81 (m, 4H), 1.09 (m, 12H), 0.78 (t, J = 7.1 Hz, 6H), 0.58 (s, 4H) ppm.

5-(4-Bromophenyl)-1*H*-tetrazole

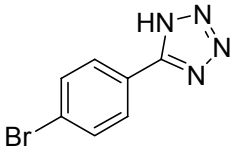

4-Bromobenzonitrile (5.00 g, 27.5 mmol), sodium azide (2.14 g, 33.0 mmol) and ammonium chloride (1.76 g, 33.0 mmol) were combined in a flame dried flask. Anhydrous DMF was added to the dry reagents and the mixture was heated at 105 °C for 12 h. The reaction mixture was allowed to cool to room temperature and was then poured onto cold water and acidified to pH 3 with dilute HCl to precipitate a white solid. The solid was filtered and washed with water to afford 5-(4-bromophenyl)-1*H*-tetrazole as a white solid (4.79 g, 77%). The NMR data were consistent with the literature.[2] ^{1}H NMR ($CDCl_3$, 400 MHz) 7.84 (d, J = 8.4 Hz, 2H), 7.99 (d, J = 8.4 Hz, 2H) ppm.

2-(4-Bromophenyl)-5-(4-*tert*-butylphenyl)-1,3,4-oxadiazole

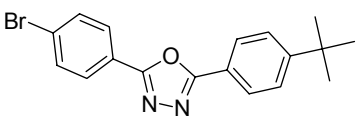

5-(4-Bromophenyl)-1*H*-tetrazole (2.11 g, 9.20 mmol) was dissolved in pyridine (30 mL) and 4-*tert*butylbenzoyl chloride (1.98 mL, 10.1 mmol). The mixture was stirred and heated to 100 °C for 3 h. The reaction mixture was then cooled and poured onto water precipitating a pale yellow solid. The solid was filtered and recrystallized from ethanol to give 2-(4-bromophenyl)-5-(4-*tert*-butylphenyl)-1,3,4-oxadiazole as white crystals (3.2 g, 92%). The NMR data were

consistent with the literature.[3] ^{1}H NMR (DMSO-d_6, 400 MHz): 8.04 (m, 4H), 7.83 (m, 2H), 7.63 (m, 2H), 1.32 (s, 9H) ppm.

9-(7-Bromo-9,9-dihexyl-9*H*-fluoren-2-yl)-9*H*-carbazole D

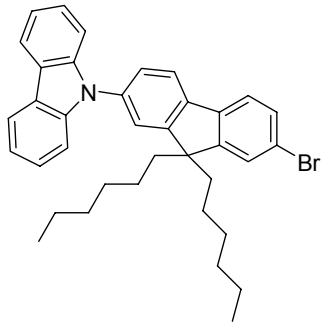

To a flame-dried flask under an atmosphere of argon 2-bromo-9,9-dihexyl-7-iodo-9*H*-fluorene (1.00 g, 1.85 mmol), carbazole (0.37 g, 2.22 mmol), copper iodide (0.03 g, 0.19 mmol), 1,10-phenanthroline (0.07 g, 0.37 mmol) and potassium carbonate (0.71 g, 3.7 mmol) were added. The flask was evacuated and backfilled with argon. Degassed DMF (8 mL) was added to the reagents *via* the septum. The mixture was stirred and heated to 120 °C for 40 h. The solvent was removed by evaporation under reduced pressure. The crude product was purified by column chromatography on silica with 98 : 2 v/v 40 – 60 petroleum ether : DCM as eluent. The product **D** was isolated as a white foamy solid (0.86 g, 80%). The NMR data were consistent with the literature.[1] ^{1}H NMR ($CDCl_3$, 700 MHz): 8.18 (d, J = 7.8 Hz, 2H), 7.88 (d, J = 7.9 Hz, 1H), 7.66 – 7.61 (m, 1H), 7.55 (m, 4H), 7.54 – 7.51 (m, 1H), 7.45 – 7.41 (m, 2H), 7.35 – 7.29 (m, 1H), 2.04 – 1.93 (m, 4H), 1.23 – 1.04 (m, 12H), 0.84 – 0.69 (m, 10H) ppm; ^{13}C NMR ($CDCl_3$, 176 MHz): 153.21, 152.21, 140.95, 139.31, 139.29, 136.81, 136.77, 130.21, 126.27, 125.91, 123.38, 121.77, 121.43, 121.21, 120.92, 120.37, 119.91, 109.70, 55.69, 40.18, 31.48, 29.55, 23.82, 22.53, 13.90.

9-(9,9-Dihexyl-7-(4,4,5,5-tetramethyl-1,3,2-dioxaborolan-2-yl)-9*H*-fluoren-2-yl)-9*H*-carbazole E

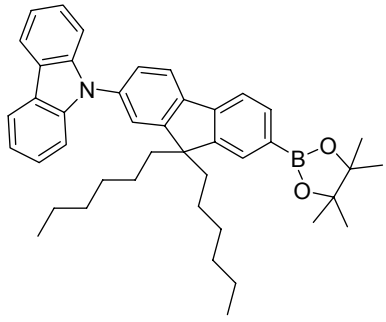

In a flame-dried flask under an atmosphere of argon **D** (1.60 g, 2.77 mmol) was dissolved in anhydrous THF (150 mL). This solution was cooled to -78 °C followed by the dropwise addition of *n*-BuLi (4.40 cm^3, 11.1 mmol). This solution was then stirred for 1 h at which time 2-isopropoxy-4,4,5,5-tetramethyl-1,3,2-dioxaborolane (2.30 mL, 11.2 mmol) was added. The reaction mixture was then stirred at room temperature for 15 h. Brine solution was then added to the mixture, which was extracted into diethyl ether. The organic phases were washed with water, dried ($MgSO_4$) and concentrated. The crude product was purified by column chromatography on silica gel with 4 : 1 v/v 40 – 60 petroleum ether : DCM as eluent. The product **E** was isolated as a foamy white solid (0.879 g, 51%); Mp 138 °C; ^{1}H NMR ($CDCl_3$, 700 MHz) δ 8.17 (d, J = 7.8

Hz, 2H), 7.97 – 7.90 (m, 1H), 7.87 (dd, *J* = 7.5 Hz, *J* = 0.9 Hz, 1H), 7.80 (s, 1H), 7.78 (dd, *J* = 7.5 Hz, *J* = 0.6 Hz, 1H), 7.56 – 7.50 (m, 2H), 7.47 – 7.39 (m, 4H), 7.31 (ddd, *J* = 7.9 Hz, *J* = 6.5 Hz, *J* = 1.5 Hz, 2H), 2.10 – 1.94 (m, 4H), 1.41 (s, 12H), 1.20 – 0.99 (m, 12H), 0.87 – 0.63 (m, 5H); ^{13}C NMR ($CDCl_3$, 176 MHz): 153.16, 150.16, 143.20, 141.00, 140.20, 136.71, 133.93, 128.90, 125.86, 125.65, 123.33, 121.81, 121.21, 120.31, 119.82, 119.14, 109.78, 83.90, 55.43, 40.12, 31.47, 30.89, 29.57, 24.94, 23.80, 22.51, 13.98 ppm; HRMS calcd for $C_{38}H_{53}{}^{10}BN_3O_4$: 625.4165. Found: 625.4183.

2-(4-(7-(9*H*-Carbazol-9-yl)-9,9-dihexyl-9*H*-fluoren-2-yl)phenyl)-5-(4-*tert*-butylphenyl)-1,3,4-oxadiazole 2

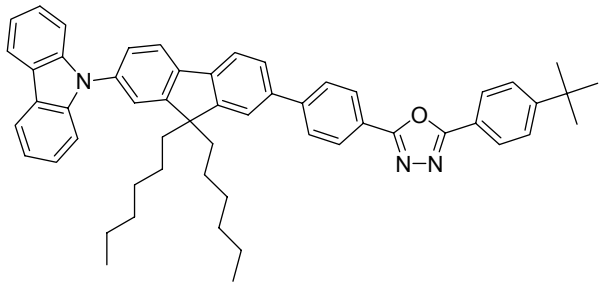

In a flame dried flask under an atmosphere of argon **E** (0.21 g, 0.33 mmol) and 2-(4-bromophenyl)-5-(4-*tert*-butylphenyl)-1,3,4-oxadiazole (0.15 g, 0.40 mmol) were combined. Anhydrous THF (30 mL) and NaOH (0.5 g in 5 mL) were added to the flask. The mixture was degassed for 1 h. To this mixture $Pd(PPh_3)_2Cl_2$ (0.14 g, 0.02 mmol) was added and the mixture was heated to reflux for 15 h. The reaction mixture was cooled, washed with brine and extracted with diethyl ether. The combined organic phases were washed with water, dried ($MgSO_4$) and concentrated. The crude product was purified by column chromatography on silica gel first with 7 : 3 v/v petroleum ether : diethyl ether, followed by DCM as eluent. The product **2** was isolated as a white solid (0.20 g, 78%); Mp: 99 °C; ^{1}H NMR (700 MHz, $CDCl_3$) δ 8.25 (d, *J* = 7.9 Hz, 2H), 8.17 (d, *J* = 7.9 Hz, 2H), 8.10 (d, *J* = 8.1 Hz, 2H), 7.95 (d, *J* = 7.9 Hz, 1H), 7.89 – 7.83 (m, 3H), 7.70 (d, *J* = 7.8 Hz, 1H), 7.66 (s, 1H), 7.60 – 7.52 (4 H, m), 7.48 – 7.38 (4 H, m), 7.31 (t, *J* = 7.2 Hz, 2H), 2.12 – 1.99 (m, 4H), 1.38 (s, 9H), 1.22 – 1.04 (m, 12H), 0.79 (dt, *J* = 20.9 Hz, *J* = 7.2 Hz, 10H) ppm; ^{13}C NMR (126 MHz, $CDCl_3$) 164.96, 164.57, 155.63, 153.16, 152.20, 144.90, 141.23, 140.75, 139.99, 139.23, 136.89, 128.03, 127.64, 127.06, 126.63, 126.34, 126.16, 126.11, 123.62, 122.94, 122.07, 121.74, 121.37, 121.32, 120.64, 120.61, 120.15, 110.02, 55.92, 40.56, 35.38, 31.75, 31.40, 29.87, 24.17, 22.87, 14.28 ppm; HRMS calcd for $C_{55}H_{57}N_3O$: 775.4502. Found: 775.4529. The ^{1}H NMR spectrum of **2** is shown in Figure S1. Purity was judged to be >99% by HPLC analysis.

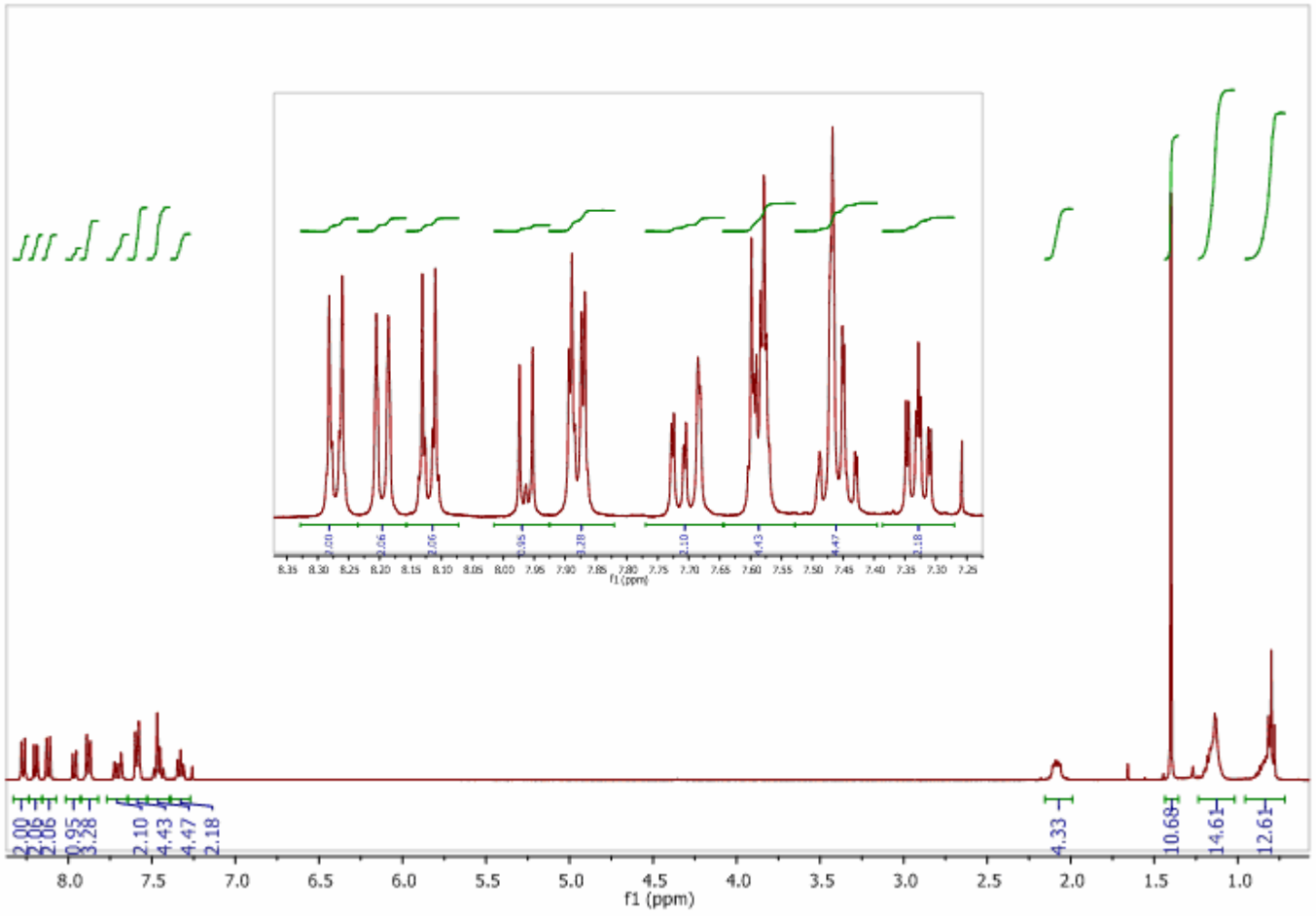

Figure S1. ^{1}H NMR spectrum of **2** in $CDCl_3$. The inset shows an expansion of the aromatic region

Cyclic Voltammetry

Cyclic voltammetry experiments were carried out using a BASCV50W electrochemical workstation in a three-electrode cell equipped with a platinum disk (*Ø* 1.6 mm) working electrode, platinum wire counter electrode and a non-aqueous Ag/Ag^+ reference electrode (0.01 M $AgNO_3$ in dry MeCN), with iR compensation. CV data for compounds **1** and **2** were obtained in dry DCM (oxidations) and dry THF (reductions) with 0.1 M tetrabutylammonium hexafluorophosphate (Bu_4NPF_6) as a supporting electrolyte, under an argon atmosphere. The potential of the reference electrode in benzonitrile (0.1 M Bu_4NPF_6) was checked against the ferrocene/ferrocenium couple (Fc/Fc^+), which showed the average potential against the reference electrode of +0.187 V.

The oxidative scans for compounds **1** and **2** are shown in Figures S2 and S3, respectively. No reduction waves could be resolved on scanning to -2.0 V.

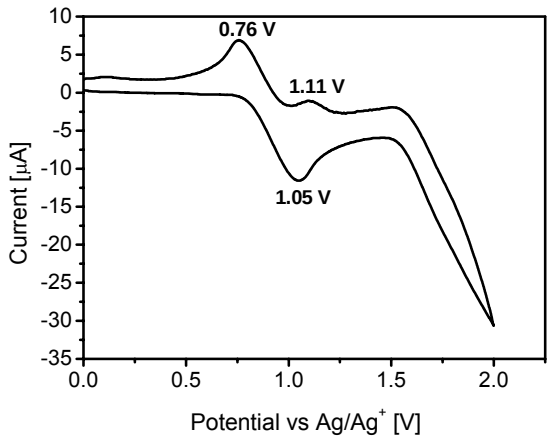

Figure S2. Oxidative scan for compound **1** in DCM

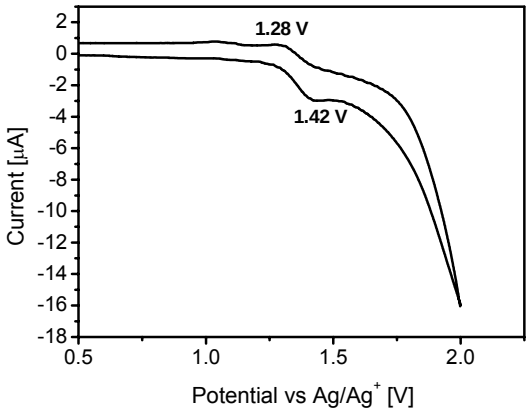

Figure S3. Oxidative scan for compound **2** in DCM

Photophysical Studies: Solution Absorption and Emission Spectra

Absorption spectra of solutions **1** and **2** in cyclohexane solution were measured in quartz cuvettes of path length l = 1 cm with an absorbance, A, < 0.3 at 400 nm using a Unicam UV2-100 spectrometer operated with the Unicam Vision software. Baseline correction was achieved by reference to pure solvent. Extinction coefficients (ε, dm^3 mol^{-1} cm^{-1}) were calculated using the Beer-Lambert law, $A = \varepsilon cl$, (c is the concentration, mol dm^{-3}) by recording the absorption spectrum for a sample weighed on an analytical balance. The excitation wavelengths for emission spectra were the absorption maxima. The spectra are shown in Figure S4.

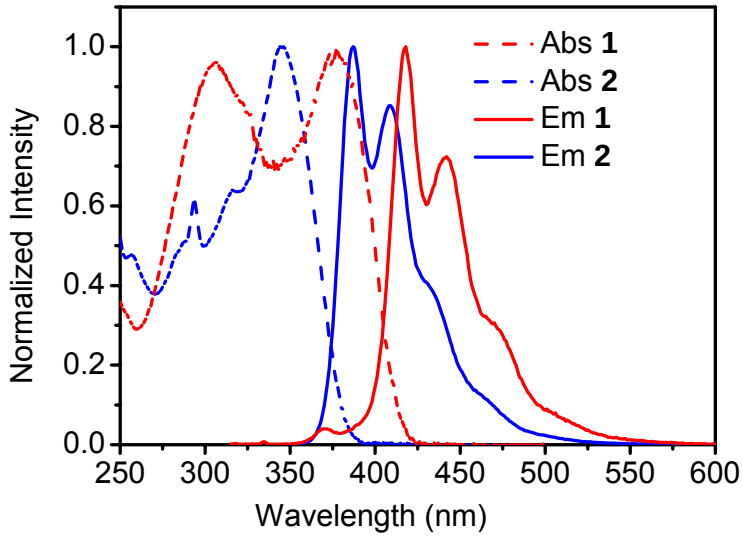

Figure S4. Absorption and emission spectra of **1** and **2** in cyclohexane solution.

Photoluminescence Spectra and Quantum Yield (PLQY) Measurements for Thin Films

Table S1. PLQY data of **1** and **2** for thin films formed by both evaporation and spin-coating.

Compound	λ_{max} (nm)	PLQY[a]
1 (Evaporated film)	467	0.30
2 (Evaporated film)	427	0.38
1 (Spin-coated film from DCM)	447	0.27
2 (Spin-coated film from DCM)	439	0.50
1 (Spin-coated film from toluene)	468	0.22
2 (Spin-coated film from toluene)	427	0.33

[a] Data obtained using an integrating sphere as described in the literature;[4] errors ±5%; excitation wavelength λ_{ex} 380 nm (compound **1**), 350 nm (compound **2**).

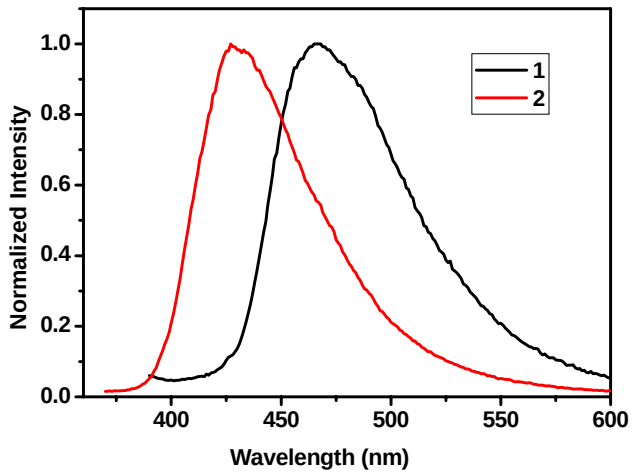

Figure S5. Photoluminescence spectra of compounds **1** and **2** from evaporated thin films.

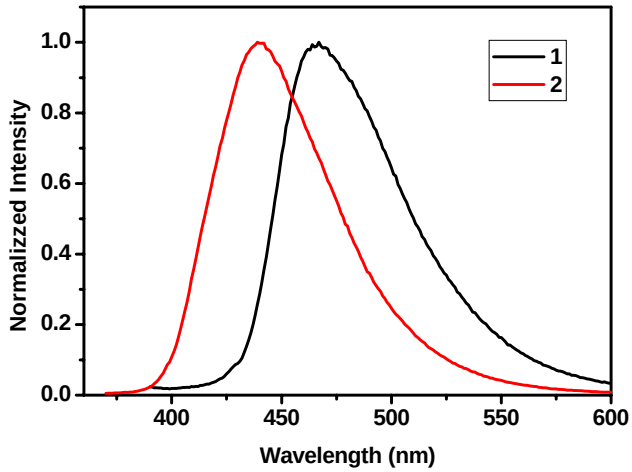

Figure S6. Photoluminescence spectra of compounds **1** and **2** from spin-coated films using DCM as a solvent.

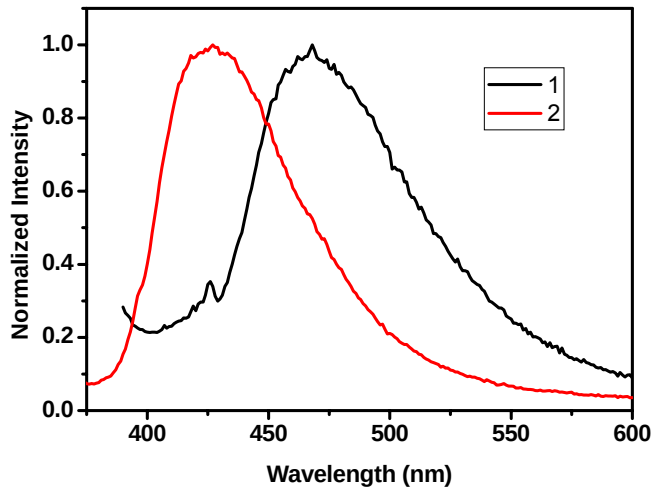

Figure S7. Photoluminescence spectra of compounds **1** and **2** from spin-coated films using toluene as a solvent.

Device Fabrication and Measurements

The OLED architecture is depicted in Figure S8. All the devices were deposited on glass substrates ready-coated with indium-tin oxide (ITO) purchased from Merck and VisionTek Systems, with a sheet resistance of 8 Ω $sq^{-1}$and 7 Ω sq^{-1}, respectively. This was used as the anode in all cases. The glass was cut to the required size and cleaned by sonication in propan-2-ol, acetone, 2% Decon 90 solution in water and finally deionized water, each for 15 min and dried

with a nitrogen gun. Poly(3,4-ethylenedioxythiophene) - poly(styrenesulfonate) (PEDOT - PSS), purchased from H. C. Starck (Clevios PVP AI 4083), was used as the hole injection layer. It was filtered through a 0.2 μm PTFE syringe filter, spin-coated at 2500 rpm for 45 seconds and dried at 180 °C for 2 min to give a layer 45 nm thick. For spin-coated **2** devices, compound **2** was dissolved in toluene (15 mg mL^{-1}) and spin-coated at 1000 rpm for 1 min to give a 70 nm thick layer. This was annealed at 80 °C for 30 min. For evaporated devices, compounds **1** and **2** were evaporated onto the PEDOT:PSS to give 70 nm and 105 nm thick layers, respectively. In both spin-coated and evaporated cases, Ca (15 nm) and Al (80 nm) electrodes with 2.5 mm radius were then thermally evaporated to complete the devices.

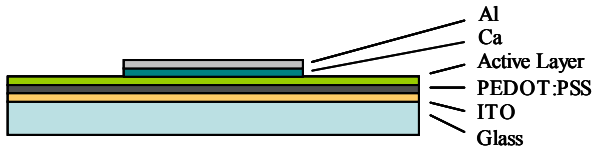

Figure S8. OLED architecture used in this work.

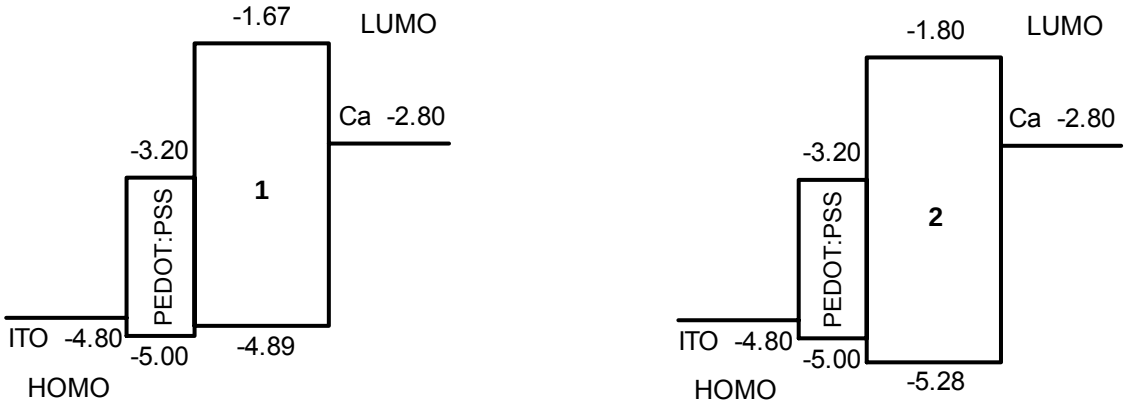

Figure S9. Device configurations showing HOMO and LUMO levels for compounds **1** and **2**.

Electrical measurements were carried out under vacuum. A D.C. bias was applied and the current was measured by a Keithley 2400 source measure unit and the light emitted from the device was collected by a large area photodiode (1.1 cm diameter) connected to a Keithley 485 digital picoammeter. For external quantum efficiency measurements, the light power was calculated using the photocurrent and the conversion factor (wavelength dependent) of the photodiode (ampere/watt). Electroluminescence spectra were recorded using an Ocean Optics USB2000 Miniature Fibre Optic Spectrometer and CIE coordinates measured using a SpectraScan PR-655 Spectroradiometer.

Figure S10 shows that the devices based on the evaporated emitters possess a significantly higher conductivity than those fabricated by spin-coating.

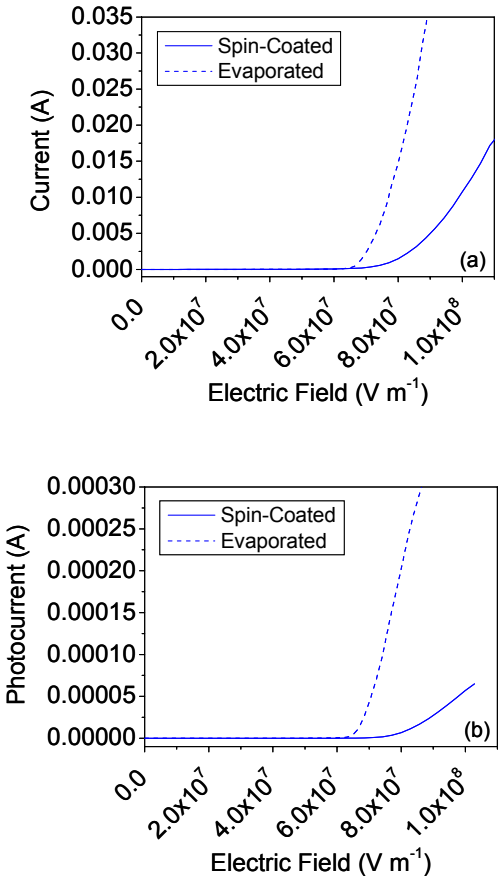

Figure S10. Comparison of the current (a) and photocurrent (b) versus electric field for spin-coated and evaporated devices of compound **2**

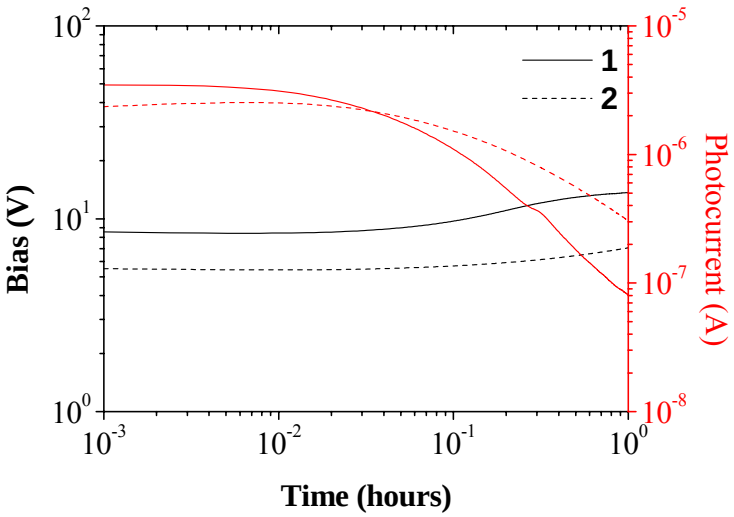

Figure S11. Comparison of the stability of evaporated devices of compounds **1** and **2** showing photocurrent versus time with changing bias.

DFT calculations

Table S2. Absorption and emission data of **1** and **2** in cyclohexane solution along with TD-DFT calculated lowest energy HOMO > LUMO transitions on optimized ground state (S_0) geometries **1a** and **2a**.

Compound	λ_{max} abs (nm)	ε (cm^{-1} mol^{-1} dm^3)	λ_{max} em (nm)	TD-DFT $S_0 > S_1$ (nm)
1 (**1a** for TD-DFT)	306, 377	31640, 32410	418, 442, 466 (sh)[a]	426
2 (**2a** for TD-DFT)	344	61510	387, 409, 431 (sh)[a]	394

[a] sh = shoulder

All computations were carried out with the Gaussian 03 package.[5] Optimized model geometries at B3LYP/6-31G* level are denoted **1a** and **2a** and contain C_2H_5 groups instead of C_6H_{13} groups in **1** and **2** respectively to reduce computational efforts. The optimized ground state (S_0) geometries have the rings coplanar with each other thereby maximizing π-π conjugation. The diphenyloxadiazole unit is planar in both cases. In reality, the systems exist as an ensemble of rotational isomers. A blue shift (ca -40 nm) and a broadening is expected in the experimental solution phase absorption spectra for **1** and **2** compared to the computed TD-DFT data listed in Table S1 for the static planar ground state geometries **1a** and **2a**. The frontier orbitals for **1a** and

2a are shown in Figures S12 and S13, respectively. The orbital energy level diagrams are shown in Figure S14.

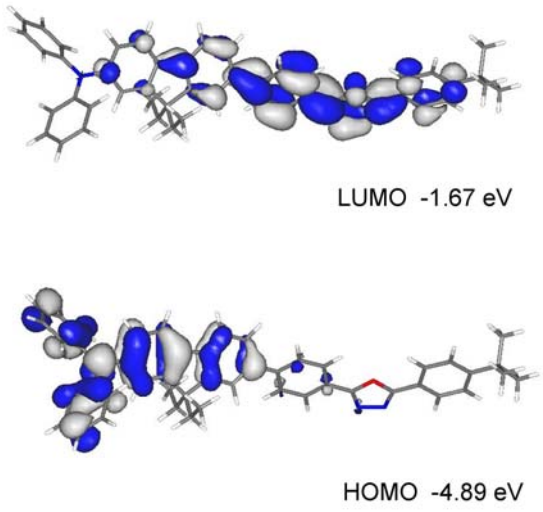

Figure S12. Frontier molecular orbitals for the optimized geometry of **1a.**

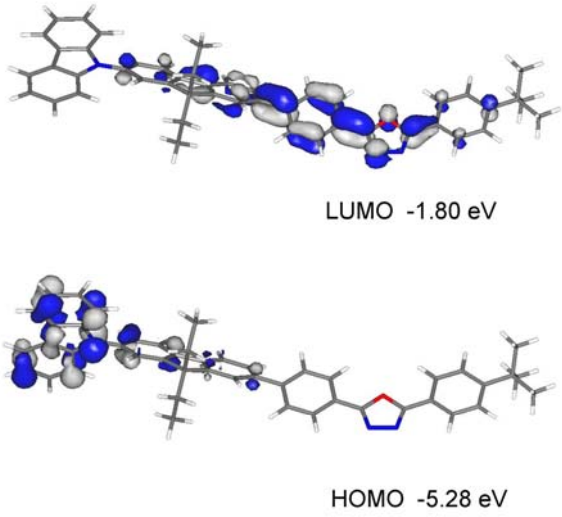

Figure S13. Frontier molecular orbitals for the optimized geometry of **2a.**

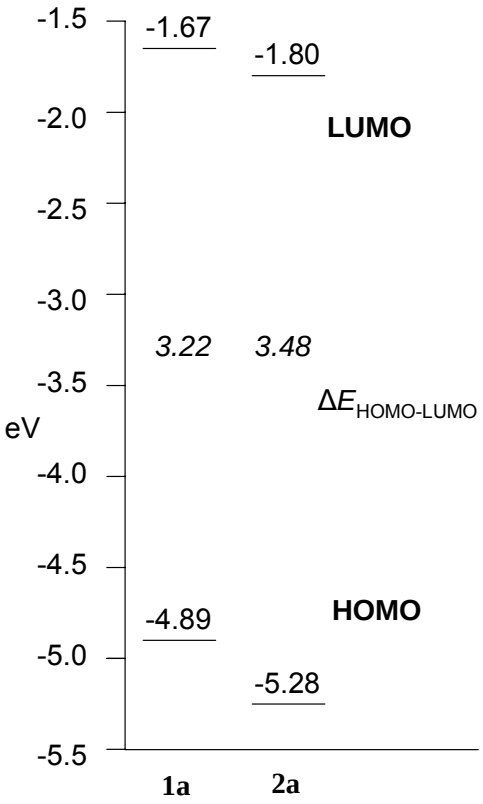

Figure S14. Orbital energy level diagrams for compounds **1a** and **2a**.

References for the Supporting Information

(1) Promarak, V.; Punkvuang, A.; Sudyoadsuk, T.; Jungsuttiwong, S.; Saengsuwan, S.; Keawin, T.; Sirithip, K. *Tetrahedron* **2007**, *63*, 8881.

(2) Hou, S.; Chan, W. K. *Macromolecules* **2001**, *35*, 850.

(3) Kamtekar, K. T.; Wang, C.; Bettington, S.; Batsanov, A. S.; Perepichka, I. F.; Bryce, M. R.; Ahn, J. H.; Rabinal, M.; Petty, M. C. *J. Mater. Chem.* **2006**, *16*, 3823.

(4) Pålsson, L.-O.; Monkman, A. P. *Adv. Mater*. **2002**, *14*, 757.

(5) Gaussian 03, Revision C.02, Frisch, M.J.; Trucks, G.W.; Schlegel, H.B.; Scuseria, G.E.; Robb, M.A.; Cheeseman, J.R.; Montgomery, Jr., J.A.; Vreven, T.; Kudin, K.N.; Burant, J.C.; Millam, J.M.; Iyengar, S.S.; Tomasi, J.; Barone, V.; Mennucci, B.; Cossi, M.; Scalmani, G.; Rega, N.; Petersson, G.A.; Nakatsuji, H.; Hada, M.; Ehara, M.; Toyota, K.; Fukuda, R.; Hasegawa, J.; Ishida, M.; Nakajima, T.; Honda, Y.; Kitao, O.; Nakai, H.; Klene, M.; Li, X.; Knox, J.E.; Hratchian, H.P.; Cross, J.B.; Adamo, C.; Jaramillo, J.; Gomperts, R.; Stratmann, R.E.; Yazyev, O.; Austin, A.J.; Cammi, R.; Pomelli, C.; Ochterski, J.W.; Ayala, P.Y.; Morokuma, K.; Voth, G.A.; Salvador, P.; Dannenberg, J.J.; Zakrzewski, V.G.; Dapprich, S.; Daniels, A.D.; Strain, M.C.; Farkas, O.; Malick, D.K.;

Rabuck, A.D.; Raghavachari, K.; Foresman, J.B.; Ortiz, J.V.; Cui, Q.; Baboul, A.G.; Clifford, S.; Cioslowski, J.; Stefanov, B.B.; Liu, G.; Liashenko, A.; Piskorz, P.; Komaromi, I.; Martin, R.L.; Fox, D.J.; Keith, T.; Al-Laham, M.A.; Peng, C.Y.; Nanayakkara, A.; Challacombe, M.; Gill, P.M.W.; Johnson, B.; Chen, W.; Wong, M.W.; Gonzalez, C.; Pople, J.A. Gaussian, Inc., Wallingford CT, 2004.